# Degradation of Diode Junction Characteristics due to Residual Defects Caused by Laser-Annealed Implantations Studied by Bipolar Test Structures

V. Gonda, T.L.M. Scholtes, and L.K. Nanver

*Abstract*—**NPN transistors are fabricated with implanted and laser annealed emitters. The transistor characteristics are compared for devices with the emitter implantation parameters varied. Results show that dectivations in the base are related to the emitter implantation dose and tilt angle. Less bulk residual implantation damage is present at low implantation doses or high tilt angles.**

*Index Terms*— **residual implantation damage, excimer laser annealing, electrical characterization**

## I. Introduction

LASER annealing of implanted dopants with short pulse melting laser processing can provide ultra-shallow and abrupt junctions with high activation levels above the solid-solubility level [1, 2]. These attractive properties are a result of the nanosecond-scale laser thermal process with $10^9$ °C/sec ramp rates and liquid-phase epitaxial regrowth. The melt depth is determined by the amorphous region formed by either the low energy implant or a pre-amorphization non-dopant implant. This type of thermal processing only affects the surface region where the melting temperature of the a-Si is reached, but in the bulk the temperature quickly drops to room temperature. For this reason, implantation damage located deeper than the amorphous/crystalline interface will not be annealed and this can have a detrimental effect on the electrical behaviour of the devices [3].

In this study we investigate the deviation of the electrical characteristics of bipolar transistors where the emitters have received an implantation that is only annealed by the laser. The effects of the residual defects on the junction properties and in the base region are investigated, and the amount and location of the damage is correlated with the implantation and laser annealing parameters. Particularly, the base-emitter leakage and the Gummel number ratios of the base are determined along with the junction capacitances. By using ring-emitter structures also the base sheet resistance is determined. In this way information is won on the dopant deactivation caused by the implantation. Moreover, the degree of junction leakage can be related to the implantation and laser annealing parameters.

Manuscript received September 27, 2006. This work was supported by the Philips PACD project.

Authors are with the Laboratory of Electronic Components, Technology, and Materials, Delft University of Technology, DIMES-ECTM, POB 5053, 2600 GB Delft, The Netherlands, (corresponding author: Viktor Gonda, tel: +31 15 278 8837, fax: +31 15 262 2163, e-mail: v.gonda@dimes.tudelft.nl).

## II. Experimental

A set of circular bipolar ring-shaped transistor structures has been designed with different ring widths [4]. The basic cross-section is shown in Fig. 1. The starting material is 4 inch (100) 2-5 Ωcm p-type silicon wafers. A buried $n^+$-layer forms the collector contact on which an undoped epitaxy layer is grown. A 30-nm thermal oxide is grown through which the $p^+$ contacts, the $n^+$-plug to the buried layer and the lightly-doped p-type base are implanted. In particularly, the base is implanted with a combination of $B^+$ implants with a total dose of $3.4 \times 10^{12}$ $cm^{-2}$ to reach a uniform concentration of $10^{17}$ $cm^{-3}$ to a depth of 300 nm. A 1050 °C 1 min thermal annealing assures the formation of ideal junctions between these implanted regions.

A laser masking stack is deposited consisting of a 300-nm-thick LPCVD TEOS surface isolation deposited at 700 °C and a 70-nm Al/Si reflective layer deposited by PVD at 50 °C. The ultra shallow and abrupt emitter $n^+$ region is fabricated by low energy implantations followed by laser annealing. The dopants are implanted in the contact windows that are first plasma etched with BHF wet landing, directly after which the excimer laser annealing (ELA) is performed. Four different 5 keV $As^+$ implanted top-gates are fabricated in the devices: the implantation dose is either 2 or $3 \times 10^{15}$ $cm^{-3}$, with tilt angles of either 7° or 30°. The latter tilt angles were combined with 8 equal rotations to avoid shadowing.

The laser annealing after the implantation was performed in a vacuum, using a commercial XMR5121 XeCl excimer laser system with a wavelength of 308 nm, pulse duration of 66 ns (full width at half maximum), single pulsed. On each wafer the laser energy densities are varied from 700 to 1150 mJ/$cm^2$ in columns. Optimal laser energies for the emitter implantations

are in the range of 900-1000 mJ/cm$^2$ [3].

The devices are completed by a standard metallization process. A 4 min HF (0.55%) dip-etch step is performed to remove the native oxide before the metallization. In this step most of the Al/Si mask is also removed. A new layer of 600 nm Al/Si(1%) is sputtered, patterned and alloyed at 400 °C for 30 min in forming gas.

The electrical characteristics were measured using an Agilent 4156C parameter analyzer, a HP 4278A capacitance meter, and a Cascade probe station.

## III. Results

Forward and reverse Gummel plots are measured to characterize the B-E junction the base region and the B-C junction in the devices having different laser annealed emitter implantations. Figure 2 shows the base current on the forward Gummel plots for various emitter implants laser annealed at 900 mJ/cm$^2$. The ideality factors are shown in Table I for all the curves measured in the low-medium current regime at 0.4 V. The emitter junction leakage can be explained by non-annealed implantation defects remains after the laser annealing in the proximity of the junction, and these defects provide extra sources of generation-recombination currents. During the implantation at least as many excess silicon interstitials are generated as the number of implanted atoms. As the laser only anneals the surface, interstitials that diffused deeper than the heat affected zone will not be annealed out. Indeed, ideality factor increases with the implantation dose as more defects are injected during the implantation. Non-idealities are slightly decreased with the increased implantation tilt angles as the less defects are directed towards the bulk.

The temperature activation of the base currents is shown in Fig. 3. The Gummel plots are measured as a function of temperature, and the only the base current is plotted. Ideality factors the currents at 0.4 V are summarized in Table II. As the temperature increases the diffusion current contribution increases over the generation-recombination current, therefore the ideality factor decreases.

The reverse Gummel plot shows the behavior of the base (by $I_E$) and base-collector junction (by $I_B$) depicted in Fig. 4. The emitter current is dependent on the base's Gummel number, and it varies due to the emitter implantation conditions. The current values are shown in Table III. Lacking of an absolute reference, the ratios of the emitter currents are a measure of the ratios of the Gummel numbers for the different implants. The base current shows near-ideal behvior, and apparently not affected by the emitter fabrication. This would be reasonable as this junction is located more than 300 nm deep from the silicon surface. However, this current was measured not to be dependent on the area of the base collector junction. This suggest that 2-D effects are prominent; the most part of the current is collected along the the ideal side of the junction which is aside of the emitter implantation window, and only a very low current flows through the part which contains defects under the emitter. In a diode measurement setup of the emitter junction when currents not forced through the damaged region, the close-to-ideal perimeter components are dominant [5].

The base is studied in more details further on. The base current is measured while it is narrowed by applying reverse bias on the emitter; at the same time the collector is kept on ground and constant negative voltage is applied on the base. The sheet conductance (or resistance) is measured by a differential measurements described in [4]. The different pinch-off shown in Fig. 5 suggest that the base width is different under the different emitters and by comparing the sheet resistances (Table III) the active base doping concentrations under the different emitter implants are different.

The active doping concentrations are determined by capacitance-voltage doping profiling and shown in Fig. 6. The active dose in the base without the shallow implants is 3.4x10$^{12}$ cm$^{-2}$ which reduces by 78% in case of a high dose emitter implant. These deactivations in the base are the results of excess silicon interstitials kicking out boron from the substitutional sites and may form boron-interstitial complexes.

## IV. Conclusion

In order to evaluate residual implantation damage after laser annealing in devices, we fabricated ring shaped NPN test structures with $As^+$ implanted and laser annealed emitters. We measured and analyzed the degradation the transistor regions under different emitter implantation parameters and optimal laser annealing. Bulk damage stemmed from non-annealed excess interstitials reaches depths larger than 300 nm under the emitter. It causes junction leakage and electrical deactivation in the regions of the transistor. The residual damage can be reduced with decreased implantation dose or tilted implants which would effectively decrease the implantation toward the bulk.


## Acknowledgment

The authors would like to thank the staff of the DIMES IC-Processing Group for their contribution to the experimental material. Special thanks to Francesco Sarubbi for the help with the capacitance measurements.

## REFERENCES

[1] Bin Yu, Yun Wang, Haihong Wang, Qi Xiang, C. Riccobene, S. Talwar, Ming-Ren Lin, "70 nm MOSFET with ultra-shallow, abrupt, and super-doped S/D extension implemented by laser thermal process (LTP)," in Proc. IEDM, pp. 509-512, 1999.

[2] L.K. Nanver, J. Slabbekoorn, A. Burtsev, T.L.M. Scholtes, R. Surdeanu, F. Simon, H.-J. Kalhert, J.W. Slotboom, "Electrical Characterization of Silicon Diodes Formed by Laser Annealing of Implanted Dopants," in Proc.ECS, Vol. 14, pp. 119-130, 2003.

[3] V. Gonda, S. Liu, T.L.M. Scholtes, L.K. Nanver, "Electrical Characterization of Residual Implantation-Induced Defects in the Vicinity of Laser-Annealed Implanted Ultrashallow Junctions", in "Doping Engineering for Device Fabrication," MRS Spring Meeting, Session C, San Francisco, CA, 2006.

[4] S. Liu, V. Gonda, T. L. M. Scholtes, L. K. Nanver, "Electrical Characterization of Residual Bulk Defects after Laser Annealing of Implanted Shallow Junctions," in Proc. IEEE-IWJT, pp. 112-115, Shanghai, China, 2006.

[5] V. Gonda, T. L. M. Scholtes, and L. K. Nanver, "The Effect of the Contact Window Edges on the Perimeter Currents of Shallow Junction Diodes," in Proc. SAFE, 2005.


TABLE I. IDEALITIY FACTORS MEASURED @0.4 V FOR EMITTERS WITH VARIOUS IMPLANTS ANNEALED AT 900 MJ/CM$^2$.

| $As^+$ implant tilt (°) dose (cm$^{-2}$) | n (-) |
|---|---|
| 7 2x10$^{15}$ | 1.34 |
| 30 2x10$^{15}$ | 1.33 |
| 30 3x10$^{15}$ | 1.36 |
| 7 3x10$^{15}$ | 1.37 |

TABLE II. TEMP VS. IDEALITY FACTOR FOR THE DEVICE IN FIG. 3 MEASURED. @0.4 V

| temperature (K) | n (-) |
|---|---|
| 260 | 1.46 |
| 280 | 1.42 |
| 300 | 1.34 |
| 320 | 1.30 |
| 340 | 1.27 |

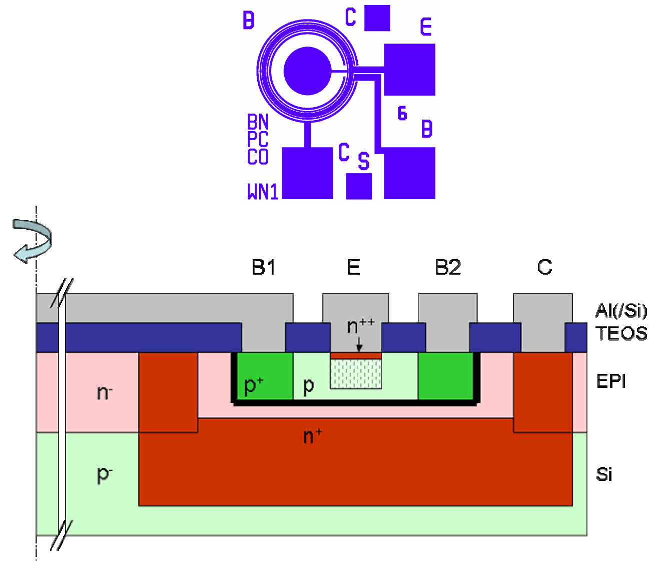


Figure 1. Ring shape device top view (top), schematic (half) cross section (bottom).

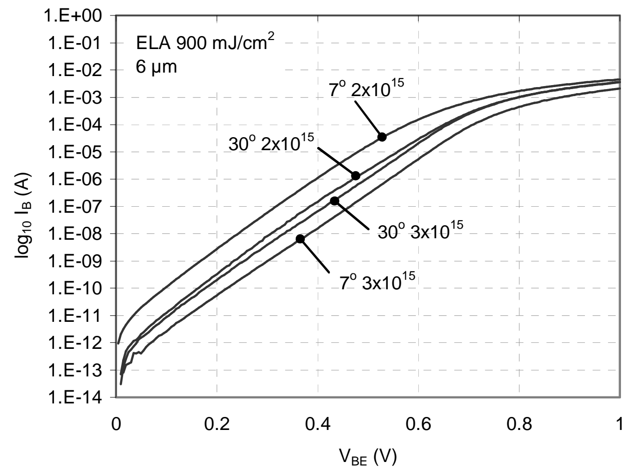


Fig. 2. The base-emitter leakage is shown by the base current on forward Gummel plots of different emitter implants laser annealed at 900mJ/cm$^2$.

TABLE III. PARAMETERS EXTRACTED FROM FIG. 4, 5, AND 6, DESCRIBING THE BASE BEHAVIOR: EMITTER CURRENT ON THE REVERSE GUMMEL PLOTS, CURRENT RATIOS (=BASE GUMMEL NUMBER RATIOS), BASE SHEET RESISTANCE, ACTIVE BORON DOSE IN THE BASE.

| 5 keV $As^+$ implant annealed @ 900 mJ/cm$^2$ tilt (°) dose (cm$^{-2}$) | $I_E$ @ 0.4V (nA) | $I_E$ ($G_B$) ratios (-) | $R_{sh}$ @ 0V (kohm/sq) | Active $B^+$ dose in base (cm$^{-2}$) | Deactivated $B^+$ dose in base (%) |
|---|---|---|---|---|---|
| 7 2x10$^{15}$ | 64.8 | } 0.97 | 23.1 | 2.13 | 37 |
| 30 2x10$^{15}$ | 66.5 | | 24.7 | 1.99 | 42 |
| 30 3x10$^{15}$ | 93.6 | } 0.61 | 40.5 | 1.21 | 64 |
| 7 3x10$^{15}$ | 153.3 | | 66.2 | 0.74 | 78 |

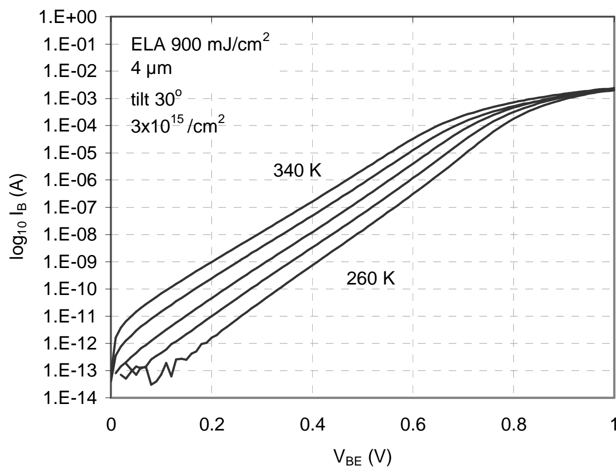


Fig. 3. The base current measured as a function of temperature from 260 to 340 K by step of 20 K.

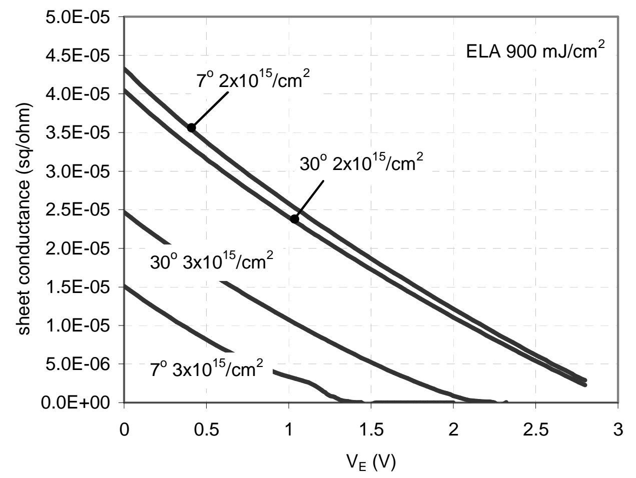


Fig. 5. Decrease of the sheet conductance of the base by pinching from the emitter.

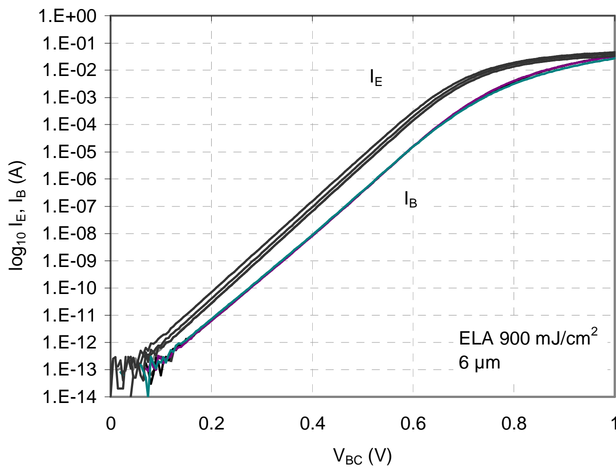


Fig. 4. Reverse Gummel plots for the different emitter implants. Current levels are summarized in Table III.

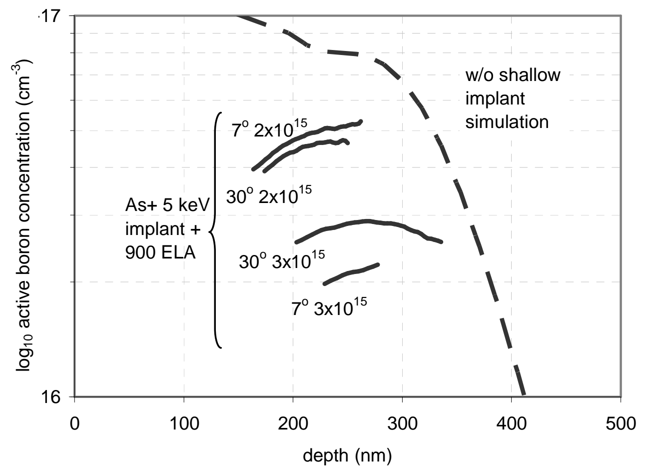


Fig. 6. Deactivations in the base after different emitter fabrication conditions. Active concentration profiles determinded by C-V profiling.